Archive of Applied Mechanics 74 (2004) 29–44 © Springer-Verlag 2004
DOI 10.1007/s00419-003-0316-3

Stress concentration of an ellipsoidal inclusion of revolution in a semi-infinite body under biaxial tension

Nao-Aki Noda, Yasuhiro Moriyama

Summary This paper deals with the stress concentration problem of an ellipsoidal inclusion of revolution in a semi-infinite body under biaxial tension. The problem is formulated as a system of singular integral equations with Cauchy-type or logarithmic-type singularities, where unknowns are densities of body forces distributed in the r- and z-directions in semi-infinite bodies having the same elastic constants as the ones of the matrix and inclusion. In order to satisfy the boundary conditions along the ellipsoidal boundary, four fundamental density functions proposed in [24, 25] are used. The body-force densities are approximated by a linear combination of fundamental density functions and polynomials. The present method is found to yield rapidly converging numerical results for stress distribution along the boundaries even when the inclusion is very close to the free boundary. The effect of the free surface on the stress concentration factor is discussed with varying the distance from the surface, the shape ratio and the elastic modulus ratio. The present results are compared with the ones of an ellipsoidal cavity in a semi-infinite body.

Keywords Stress concentration, Body-force method, Ellipsoidal inclusion, Singular integral equation, Numerical analysis, Semi-infinite body

1
Introduction

Structural materials usually contain some defects in the form of cracks, cavities, and inclusions. For various metals, the size, shape, and distribution of microdiscontinuities have been investigated e.g. in [1, 2]. To evaluate their defects on the strength, it is fundamental to know the stress concentration of elliptical and ellipsoidal inclusions, which cover many particular cases, such as linear, circular, and spherical defects. In earlier studies, ellipsoidal inclusions have been studied by several researchers, [3–6]. Also, interactions among elliptical and ellipsoidal inclusions have been discussed in [7–17]. Several elasticity problems involving a half-space with a spheroidal inclusion have been studied in [18–22]. However, there has been little discussion about ellipsoidal inclusions in a half-space.

In this study, therefore, stress concentration of an ellipsoidal inclusion of revolution in a semi-infinite body under bi-axial tension is considered. An ellipsoidal inclusion can be regarded as a general model of the defect because many kinds of defects can be expressed by changing the elastic modulus ratio and the shape ratio of the inclusion. The body-force method, [23], is used here to formulate the problem as a system of singular integral equations. Then, the unknown body-force densities are approximated by a linear combination of fundamental density functions and polynomials [24–26]. The results will be compared with the ones in [18–22] by setting the elastic modulus of the inclusion $E_I = 0$, see Fig. 1. It will be shown that the present method gives smooth variations of interface stresses along the boundary.

2
Analysis and numerical procedure

Consider a semi-infinite body under biaxial tension having an ellipsoidal inclusion as shown in Fig. 1. The body force method is used to formulate the problem as a system of singular integral

Received 14 January 2003; accepted for publication 11 November 2003

N.-A. Noda (✉), Y. Moriyama
Department of Mechanical Engineering,
Kyushu Institute of Technology,
Kitakyushu 804–8550, Japan
e-mail: noda@mech.kyutech.ac.jp

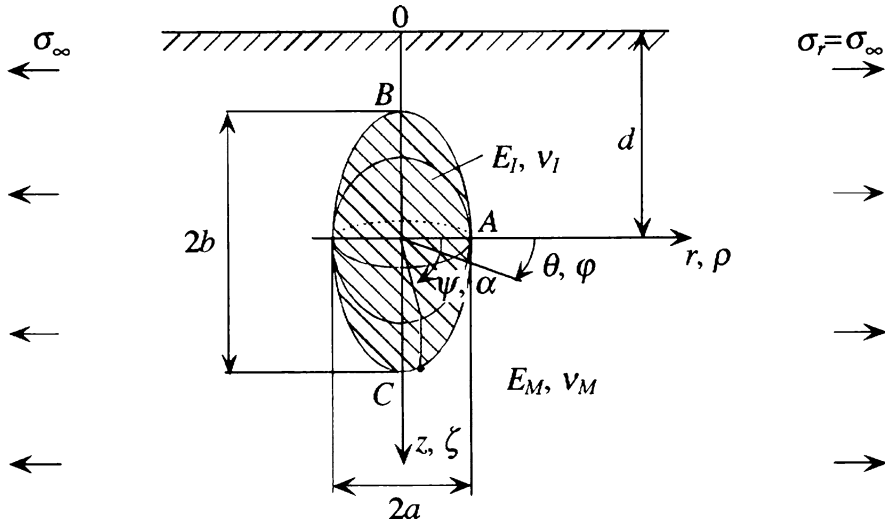

Fig. 1. An ellipsoidal inclusion in a semi-infinite body under biaxial tension

equations. In this analysis fundamental solutions are stress (K_{nn}^{Fr}, K_{nn}^{Fz}, K_{nt}^{Fr}, K_{nt}^{Fz}) and displacement fields (K_{ur}^{Fr}, K_{ur}^{Fz}, K_{uz}^{Fr}, K_{uz}^{Fz}) at an arbitrary point (r, θ, z) when ring forces are acting in the r- and z-directions at (ρ, φ, ζ) in a semi-infinite body. Here, (ρ, φ, ζ) is a point in the (r, θ, z) coordinate system, where ring forces are applied:

$$\rho = a\cos\alpha, \quad \zeta = d + b\sin\alpha, \quad r = a\cos\psi, \quad z = d + b\sin\psi.$$

A semi-infinite body "M" and an infinite body "I" are considered, each of which having the same elastic constants as those of the matrix (E_M, ν_M) and the inclusion (E_I, ν_I). Denote by σ_{nM}, τ_{ntM}, u_{rM}, u_{zM} the stresses and displacements which appear along the prospective elliptical boundaries in the semi-infinite body "M". In a similar way, denote by σ_{nI}, τ_{ntI}, u_{rI}, u_{zI} the stresses and displacements which appear along the prospective elliptical boundaries in the infinite body "I". Then, the boundary conditions, that is

$$\sigma_{tM} - \sigma_{tI} = 0,\ \tau_{ntM} - \tau_{ntI} = 0,\ u_{rM} - u_{rI} = 0,\ u_{zM} - u_{zI} = 0,$$

can be expressed as

$$\begin{aligned}
&-\frac{1}{2}\left\{\rho_{rM}^*(\psi)\cos\psi_0 + \rho_{zM}^*(\psi)\sin\psi_0\right\} - \frac{1}{2}\left\{\rho_{rI}^*(\psi)\cos\psi_0 + \rho_{zI}^*(\psi)\sin\psi_0\right\} \\
&\quad + \int_{-\pi/2}^{\pi/2} K_{nnM}^{Fr}(\alpha,\psi)\rho_{rM}^*(\alpha)ds + \int_{-\pi/2}^{\pi/2} K_{nnM}^{Fz}(\alpha,\psi)\rho_{zM}^*(\alpha)ds \\
&\quad - \int_{-\pi/2}^{\pi/2} K_{nnI}^{Fr}(\alpha,\psi)\rho_{rI}^*(\alpha)ds - \int_{-\pi/2}^{\pi/2} K_{nnI}^{Fz}(\alpha,\psi)\rho_{zI}^*(\alpha)ds \\
&\quad = -\left(\sigma_z^\infty \sin^2\psi_0 + \sigma_r^\infty \cos^2\psi_0\right), \\
&\quad \frac{1}{2}\left\{\rho_{rM}^*(\psi)\sin\psi_0 - \rho_{zM}^*(\psi)\cos\psi_0\right\} + \frac{1}{2}\left\{\rho_{rI}^*(\psi)\sin\psi_0 - \rho_{zI}^*(\psi)\cos\psi_0\right\} \\
&\quad + \int_{-\pi/2}^{\pi/2} K_{ntM}^{Fr}(\alpha,\psi)\rho_{rM}^*(\alpha)ds + \int_{-\pi/2}^{\pi/2} K_{ntM}^{Fz}(\alpha,\psi)\rho_{zM}^*(\alpha)ds \\
&\quad - \int_{-\pi/2}^{\pi/2} K_{ntI}^{Fr}(\alpha,\psi)\rho_{rI}^*(\alpha)ds - \int_{-\pi/2}^{\pi/2} K_{ntI}^{Fz}(\alpha,\psi)\rho_{zI}^*(\alpha)ds \\
&\quad = -\left(\sigma_z^\infty - \sigma_r^\infty\right)\sin\psi_0\cos\psi_0,
\end{aligned} \tag{1}$$

$$\int_{-\pi/2}^{\pi/2} K_{urM}^{Fr}(\alpha,\psi)\rho_{rM}^{*}(\alpha)ds + \int_{-\pi/2}^{\pi/2} K_{urM}^{Fz}(\alpha,\psi)\rho_{zM}^{*}(\alpha)ds$$
$$- \int_{-\pi/2}^{\pi/2} K_{urI}^{Fr}(\alpha,\psi)\rho_{rI}^{*}(\alpha)ds - \int_{-\pi/2}^{\pi/2} K_{urI}^{Fz}(\alpha,\psi)\rho_{zI}^{*}(\alpha)ds$$
$$= -\left\{\sigma_r^{\infty} - \nu_M\left(\sigma_\theta^{\infty} + \sigma_z^{\infty}\right)\right\} r/E_M,$$
$$\int_{-\pi/2}^{\pi/2} K_{uzM}^{Fr}(\alpha,\psi)\rho_{rM}^{*}(\alpha)ds + \int_{-\pi/2}^{\pi/2} K_{uzM}^{Fz}(\alpha,\psi)\rho_{zM}^{*}(\alpha)ds$$
$$- \int_{-\pi/2}^{\pi/2} K_{uzI}^{Fr}(\alpha,\psi)\rho_{rI}^{*}(\alpha)ds - \int_{-\pi/2}^{\pi/2} K_{uzI}^{Fz}(\alpha,\psi)\rho_{zI}^{*}(\alpha)ds$$
$$= -\left\{\sigma_z^{\infty} - \nu_M\left(\sigma_r^{\infty} + \sigma_\theta^{\infty}\right)\right\} z/E_M, \tag{2}$$

where

$$\frac{-\pi}{2} \le \psi \le \frac{\pi}{2},\ -d\rho = a\sin\alpha d\alpha,\ d\zeta = b\cos\alpha d\alpha,\ ds = \sqrt{a^2\sin^2\alpha + b^2\cos^2\alpha}\,d\alpha,$$

and ψ_0 is the angle between the r-axis and the normal direction of an ellipsoidal inclusion at (r, z). The unknowns are the body force densities $\rho_{rM}^{*}(\alpha)$, $\rho_{zM}^{*}(\alpha)$, $\rho_{rI}^{*}(\alpha)$, $\rho_{zI}^{*}(\alpha)$ distributed in the bodies M and I in the r- and z- directions along the circumference, which is specified by the angle α.

Equation (1) includes Cauchy-type singular terms, and Eq. (2) includes logarithm-type singular terms. Therefore for Eq. (1) the integral should be taken in a sense of Cauchy' s of principal value when $\psi = \alpha$. The first and second terms of Eq. (1) represent the stress due to the body force distributed on the imaginary boundary, which is composed of the internal or external points that are infinitesimally apart from the initial boundary, [23]. Taking $K_{nnM}^{Fr}(\alpha,\psi)$ for example, the notation means the normal stress σ_{nM} induced at the point where a ring force in the r-direction is acting on the imaginary boundary in the body "M". These can be derived by integrating Mindlin's solution, [27], in the θ-direction. The fundamental stress and displacement fields are shown in the Appendix, where ring forces are acting in the r- and z-directions in a semi-infinite body.

In previous papers, [24, 25], numerical solutions for the singular integral equations of the body-force method were discussed. It was found that in the conventional body-force method, unknown body-force densities sometimes do not converge with increasing the number of collocation points. To overcome this difficulty, eight fundamental densities were introduced in [24, 25]. The meaning of the new fundamental densities was discussed in [26]. On the basis of these studies, the unknown body-force densities are approximated in this analysis as a linear combination of fundamental density functions and weight functions as follows:

$$\rho_{rM}^{*}(\alpha) = \rho_{r3M}(\alpha)w_{r3}(\alpha) + \rho_{r4M}(\alpha)w_{r4}(\alpha),$$
$$\rho_{zM}^{*}(\alpha) = \rho_{z1M}(\alpha)w_{z1}(\alpha) + \rho_{z2M}(\alpha)w_{z2}(\alpha),$$
$$\rho_{rI}^{*}(\alpha) = \rho_{r3I}(\alpha)w_{r3}(\alpha) + \rho_{r4I}(\alpha)w_{r4}(\alpha),$$
$$\rho_{zI}^{*}(\alpha) = \rho_{z1I}(\alpha)w_{z1}(\alpha) + \rho_{z2I}(\alpha)w_{z2}(\alpha). \tag{3}$$

Here, the fundamental density functions, [24, 25], are defined as

$$w_{r3}(\alpha) = n_r(\alpha), w_{r4}(\alpha) = n_r(\alpha)\sin\alpha,$$
$$w_{z1}(\alpha) = \frac{n_z(\alpha)}{\sin\alpha}, w_{z4}(\alpha) = n_z(\alpha), \tag{4}$$

with

$$n_r(\alpha) = \frac{b\cos\alpha}{\sqrt{a^2\sin^2\alpha + b^2\cos^2\alpha}},$$
$$n_z(\alpha) = \frac{a\sin\alpha}{\sqrt{a^2\sin^2\alpha + b^2\cos^2\alpha}}. \tag{5}$$

In these equations, $w_{r3}(\alpha)$, $w_{z2}(\alpha)$ are exact densities to express the stress field due to an ellipsoidal inclusion in an infinite body.
On the other hand, the weight functions are approximated by polynomials as:

$$\rho_{r2M}(\alpha) = \sum_{n=1}^{M/2} a_{nM}t_n(\alpha), \rho_{r2I}(\alpha) = \sum_{n=1}^{M/2} a_{nI}t_n(\alpha),$$
$$\rho_{z1M}(\alpha) = \sum_{n=1}^{M/2} c_{nM}t_n(\alpha), \rho_{z1I}(\alpha) = \sum_{n=1}^{M/2} c_{nI}t_n(\alpha),$$
$$\rho_{r4M}(\alpha) = \sum_{n=1}^{M/2} b_{nM}t_n(\alpha), \rho_{r4I}(\alpha) = \sum_{n=1}^{M/2} b_{nI}t_n(\alpha),$$
$$\rho_{z2M}(\alpha) = \sum_{n=1}^{M/2} d_{nM}t_n(\alpha), \rho_{z2I}(\alpha) = \sum_{n=1}^{M/2} d_{nI}t_n(\alpha).$$
$$t_n(\alpha) = \cos\{2(n-1)\alpha\}. \tag{6}$$

where M is the number of the collocation points in the range $-\pi/2 \le \alpha \le \pi/2$.

Using the approximation method mentioned above, we obtain the following system of linear equations for the determination of the coefficients $a_{nM} \sim d_{nI}$:

$$\theta_L = \frac{\pi}{M}(L - 0.5) - \frac{\pi}{2} \quad 2 \le L \le M, \tag{7}$$

$$\sum_{n=1}^{M/2} \left(a_{nM}A_{nM} + b_{nM}B_{nM} + c_{nM}C_{nM} + d_{nM}D_{nM} + a_{nI}A_{nI} + b_{nI}B_{nI} + c_{nI}C_{nI} + d_{nI}D_{nI}\right) = -\left(\sigma_z^\infty \sin^2\varphi_0 + \sigma_r^\infty \cos^2\varphi_0\right), \tag{8}$$

$$\sum_{n=1}^{M/2} \left(a_{nM}E_{nM} + b_{nM}F_{nM} + c_{nM}G_{nM} + d_{nM}H_{nM} + a_{nI}E_{nI} + b_{nI}F_{nI} + c_{nI}G_{nI} + d_{nI}H_{nI}\right) = -\left(\sigma_z^\infty - \sigma_r^\infty\right)\sin\varphi_0\cos\varphi_0, \tag{9}$$

$$\sum_{n=1}^{M/2} \left(a_{nM}I_{nM} + b_{nM}J_{nM} + c_{nM}K_{nM} + d_{nM}L_{nM} + a_{nI}I_{nI} + b_{nI}J_{nI} + c_{nI}K_{nI} + d_{nI}L_{nI}\right) = -\left\{\sigma_r^\infty - v_M\left(\sigma_\theta^\infty + \sigma_z^\infty\right)\right\}r/E_M, \tag{10}$$

$$\sum_{n=1}^{M/2} \left(a_{nM}M_{nM} + b_{nM}N_{nM} + c_{nM}O_{nM} + d_{nM}P_{nM} + a_{nI}M_{nI} + b_{nI}N_{nI} + c_{nI}O_{nI} + d_{nI}P_{nI}\right) = -\left\{\sigma_z^\infty - v_M\left(\sigma_r^\infty + \sigma_\theta^\infty\right)\right\}z/E_M, \tag{11}$$

Table 1. Convergence of the interface stresses at $\psi = -90$, comp. Fig. 1, (a/b = 1, b/d = 0.9, $E_I/E_M = 2$, $\nu_M = \nu_I = 0.3$)

M	σ_{tM}	σ_{tI}	σ_{nM}	σ_{nI}	τ_{ntM}	τ_{ntI}
8	0.5247	1.5997	0.1448	0.1976	0.0128	0.0132
12	0.5080	1.5539	0.1451	0.1376	0.0132	0.0131
20	0.5024	1.5530	0.1396	0.1395	0.0130	0.0130
22	0.5024	1.5530	0.1396	0.1396	0.0130	0.0130

Table 2. Mismatch of the boundary stresses and displacements at $\psi = -90$ (a/b = 1, b/d = 0.9, $E_I/E_M = 2$, $\nu_M = \nu_I = 0.3$)

M	$\sigma_{tM} - \sigma_{tI}$	$\tau_{ntM} - \tau_{ntI}$	$u_{rM} - u_{rI}$	$u_{zM} - u_{zI}$
8	-5.3×10^{-2}	-3.6×10^{-4}	-3.9×10^{-5}	6.3×10^{-3}
12	7.6×10^{-3}	-2.1×10^{-4}	-1.0×10^{-5}	5.8×10^{-4}
20	1.1×10^{-4}	1.4×10^{-5}	-2.7×10^{-7}	5.3×10^{-7}
22	-6.1×10^{-6}	1.1×10^{-5}	3.4×10^{-8}	3.7×10^{-7}

Table 3. Stress concentration factor of two spheroidal cavities in an infinite body (a/b = 1.0), comp. Fig. 2

a/d	$\sigma_{\theta\max}$		K_{tA}	K_{tB}
	(deg.)	K_{tmax}		
0	−90∼+90	2.0455	2.0455	2.0455
0.1	−2	2.0455	2.0454	2.0454
0.2	−10	2.0462	2.0448	2.0454
0.3	−14	2.0481	2.0427	2.0456
0.4	−17	2.0521	2.0378	2.0464
0.5	−24	2.0598	2.0307	2.0481
0.6	−31	2.0742	2.0295	2.0512
0.7	−41	2.1022	2.0655	2.0561
0.8	−90	2.2295	2.2295	2.0624
0.9	−90	2.7724	2.7724	2.0713

$$A_{nM} = -\frac{1}{2} t_n(\varphi) \cos^2 \varphi_0 + \int_{-\pi/2}^{\pi/2} K_{nnM}^{Fr}(\alpha, \varphi) t_n(\varphi) b \cos \alpha d\alpha. \tag{12}$$

The number of unknown coefficients is 4 M. The collocation points are set as given by Eq. (7). The stresses at an arbitrary point are represented by a linear combination of the coefficients $a_{nM}, \ldots, d_{nI}$ and the influence coefficients corresponding to $A_{nM}, \ldots, P_{nI}$, [25, 26]. Using the numerical procedure presented above, we obtain the stress distribution along the interface and will discuss the maximum stress in Sec 3.

3
Results and discussion

3.1
Convergence and satisfaction of the boundary stresses

Table 1 shows the convergence of interface stresses σ_{tM}, σ_{nM}, τ_{ntM}, σ_{tI}, σ_{nI}, τ_{ntI} at $\psi = -90$, comp. Fig. 1, with increasing values of the collocation number M. Table 2 shows the mismatch of the boundary values: $\sigma_{tM} - \sigma_{tI}$, $\tau_{ntM} - \tau_{ntI}$, $u_{rM} - u_{rI}$, $u_{zM} - u_{zI}$ at $\psi = -90$ with increasing number M. The present results show good convergence to the fifth digit when $M = 20$. Also the boundary mismatch values are confirmed to be less than 10^{-4} in the whole range $-90 \leq \psi \leq 90$. The same examination has been made for other calculations. Good convergence and high matching of boundary values are confirmed for all results with $E_I/E_M(0 - \infty)$, and b/d in the range (0–0.9).

The accuracy of the present analysis can be confirmed in Table 3. Here, two spheroidal cavities in an infinite body under uniaxial tension, see Fig. 2, were treated by the same method

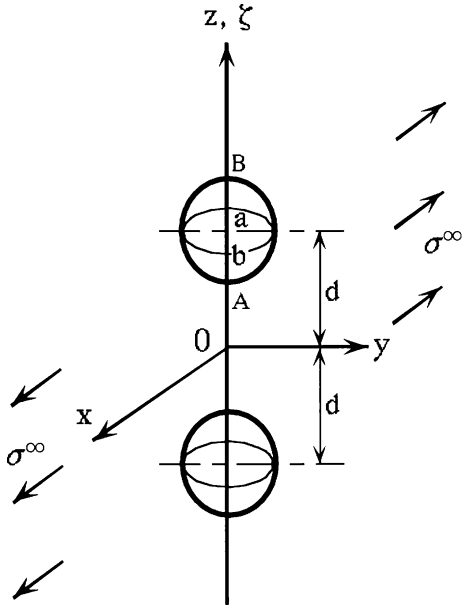

Fig. 2. Two spheroidal cavities in an infinite body ($a/b = 1.0$)

and compared with the results in [15]. Both results coincide with each other to the fourth digit. However, the present solution gives the accurate results even for $a/d = 0.9$ where larger interaction takes now.

3.2
Results for a spheroidal cavity ($E_I/E_M = 0$, $a/b = 1$)

Table 4 shows the maximum stress in comparison with the results in [20] for different ratios b/d. Here, the maximum stress $\sigma_t = \sigma_\theta$ appearing at the point B ($\psi = -90$) is indicated. The results in [20] coincide with the present results in most cases although they have some error of about 3% when $b/d = 0.9$.

3.3
Results of an ellipsoidal cavity ($E_I/E_M = 0$)

Table 5 shows the maximum stress when $v_M = 0.3$, for different shape ratios a/b and different ratios b/d. The results in [21] coincide with the present results in most cases although they have some errors about 2% when $a/b = 1, b/d = 0.667$. Table 6 shows the stress ($\sigma_t = \sigma_\theta$) at points B ($\psi = -90$) and C ($\psi = 90$) for different a/b and b/d. It is found that results [21] have errors within about 11% when $b/d = 0.8$. The present results are reliable because the boundary conditions are satisfied as shown in Table 2.

3.4
Results for an ellipsoidal inclusion

If $E_I/E_M < 1$, interface stresses σ_θ in the matrix need to be considered because they are larger than other stresses. Also, if $E_I/E_M > 1$, interface stresses σ_n have to be discussed because they may cause interface debonding. Figures 3–5 show interface stresses σ_θ ($E_I/E_M = 0; 0.5$) and σ_n ($E_I/E_M = 2; \infty$) for different ratios a/b and b/d. It is seen that when $E_I/E_M = 0.5$ the effect of

Table 4. Maximum stress due to a spheroidal cavity at B, comp. Fig. 1 ($E_I/E_M = 0$, $v_M = 0.25$, $a/b = 1$, $\psi = -90$)

b/d	Present	Ref [20]
0	2.087	2.087
0.2	2.092	2.092
0.4	2.145	2.145
0.6	2.332	2.332
0.7	2.506	2.506
0.8	2.759	2.760
0.9	3.173	3.270

Table 5. Maximum stress due to ellipsoidal cavities at B, comp. Fig. 1 ($E_I/E_M = 0$, $v_M = 0.3$, $\psi = -90$)

b/d	a/b	0.286	0.333	0.4	0.5	0.667	1.0
0.333	Present	2.713	2.679	2.624	2.545	2.420	2.216
	Ref [21]	2.712	2.671	2.624	2.544	2.425	2.227
0.4	Present	2.715	2.680	2.629	2.552	2.434	2.245
	Ref [21]	2.714	2.674	2.627	2.550	2.434	2.245
0.5	Present	2.732	2.690	2.643	2.575	2.471	2.326
	Ref [21]	2.724	2.689	2.648	2.583	2.488	2.350
0.667	Present	2.755	2.731	2.701	2.663	2.620	2.581
	Ref [21]	2.753	2.740	2.716	2.686	2.651	2.618

Table 6. Maximum stress due to ellipsoidal cavities at B, comp. Fig. 1 ($\psi = -90$) and C ($\psi = 90$) ($E_I/E_M = 0$, $v_M = 0.3$)

b/d	a/b ψ(deg.)	0.25		0.5	
		$-90°$	$90°$	$-90°$	$90°$
0	Present	2.737	2.737	2.536	2.536
	Ref. [21]	–	–	–	–
0.2	Present	2.738	2.737	2.538	2.537
	Ref. [21]	2.741	2.740	2.539	2.538
04	Present	2.749	2.729	2.552	2.540
	Ref. [21]	2.744	2.741	2.553	2.541
0.6	Present	2.808	2.687	2.617	2.541
	Ref. [21]	2.758	2.742	2.615	2.544
0.8	Present	3.169	2.429	2.829	2.539
	Ref. [21]	2.810	2.743	2.829	2.547
0.9	Present	4.777	1.210	3.104	2.535
	Ref. [21]	–	–	–	–

free surface is comparatively smaller than the case of $E_I/E_M = 0$. With increasing b/d, the stress σ_n generally increases near $\psi = -90$; however, when $b/d \to 1$, stress distribution near $\psi = -90$ becomes complicated due to the effect of free surface, S. e.g., $b/d = 0.9$ in Fig. 4 (b). Also, it is found that the maximum stress σ_n at $\psi = 0$ is almost independent of b/d, although the stress in the range $\psi \leq -30$ varies largely, depending on b/d.

Table 7 shows the magnitude and position of the maximum stress in the matrix . As shown in Table 7, the maximum stresses σ_θ appear at $\psi = \pm 90$ in most cases. On the other hand, the maximum stresses σ_n appear at $\psi = 0$. With increasing value of b/d, the maximum stresses increases when $E_I/E_M = 0$, 0.5. However, when $b/d \to 1$, the maximum stresses sometimes become smaller. Also maximum stress sometimes appears near $\psi = -70$, instead $\psi = -90$. When $E_I/E_M < 1$, the maximum stress σ_θ varies more than twice in the range $b/d = 0 - 0.9$. On the other hand, when $E_I/E_M > 1$, the variation of the maximum stress σ_θ is only 8% at the most. When $E_I/E_M > 1$, the effect of the free surface is comparatively small because the maximum stress appears at $\psi = 0$.

Recently, in paper [28] by using inclusion models of MnS and Al_2O_3 in the matrix it was explained why the S-N curve for high-strength steels consists of two straight lines. The FEM analysis indicated that in rotating-fatigue tests fracture is likely to occur from a surface origin at high stress level and from an internal inclusion at low stress level. Figure 6 shows the stress concentration due to a spheroidal inclusion in an infinite body under uniaxial and biaxial tension. Also, Table 8 with Fig. 7 shows the maximum stress due to the inclusions in a semi-infinite body under biaxial tension. In Figs. 6, 7 and Table 8 we assume the following data, [29]: matrix of high strength steel: $E_M = 210$ GPa, v_M=0.3; MnS : $E_I = 100$ GPa, $v_I = 0.3$; Al_2O_3 : $E_I = 400$ GPa, $v_I = 0.25$; aspect ratio of the inclusion: $a/b = 1$

As shown in Table 8, it is seen that the variation of the maximum stress is less than 7% in the range $b/d = 0 - 0.9$. The effect of the free surface is not very large in this region under uniform biaxial tension.

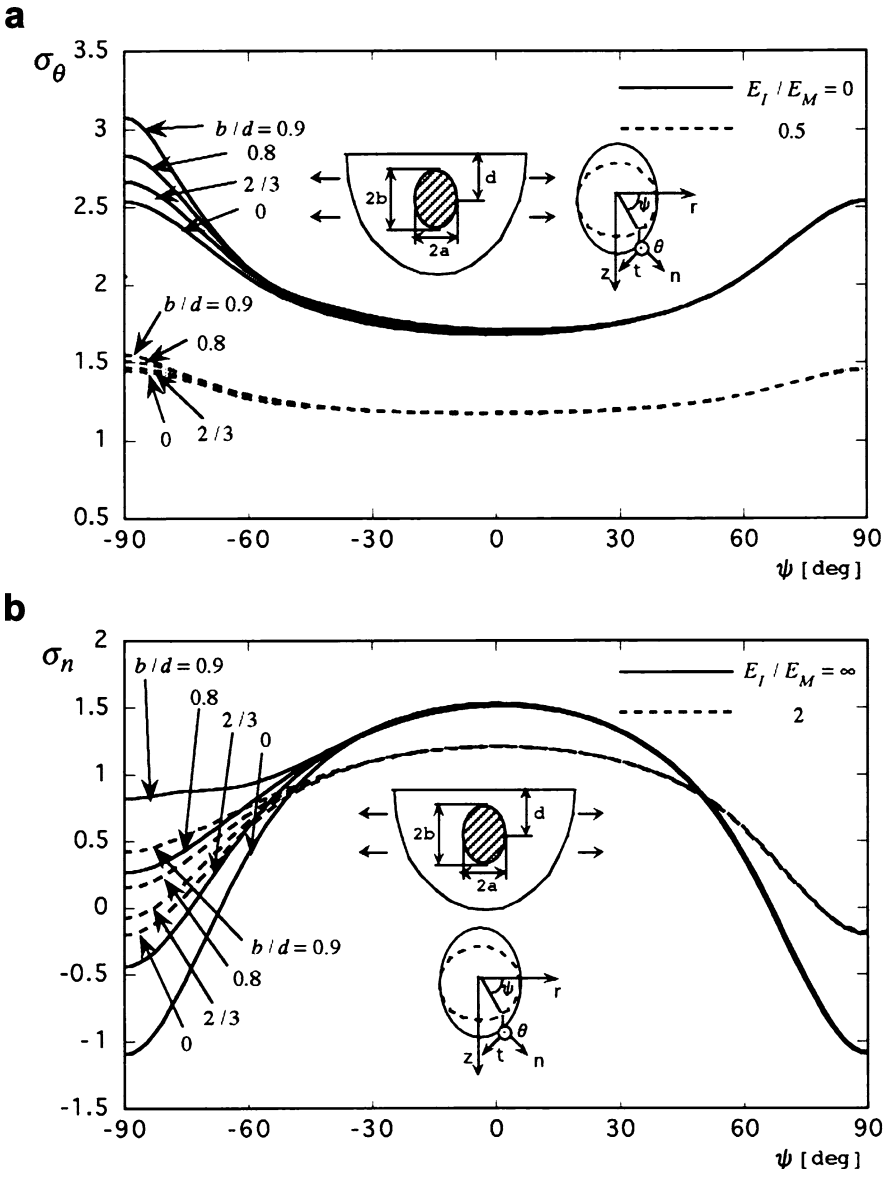

Fig. 3a, b. Interface stress for $a/b = 1/2$ **(a)** σ_θ for $E_I/E_M < 1$; **(b)** σ_n for $E_I/E_M > 1$

4 Conclusions

In this study, an ellipsoidal inclusion of revolution in a semi-infinite body under biaxial tension is considered using the body-force method. The following conclusions can be made:

1) The problem is solved using the body-force method coupled with a singular integral equations formulation. In order to satisfy the boundary conditions, the unknown functions are approximated by a linear combination of fundamental density functions and polynomials. The present method is found to yield rapidly converging numerical results and smooth stress distribution along the boundary (s. Tables 1, 2).
2) Expressions for stresses and displacements ring forces acting in the r- and z-directions in a semi-infinite body can be used as a fundamental solution for the body-force method and boundary element method (s. Appendix).
3) For spheroidal inclusions of MnS and Al_2O_3 in high strength steel, the effect of free surface on the stress concentration is found to be not very large (s. Table 8). For ellipsoidal cavities ($E_I/E_M = 0$), the present results coincide with those of [20] in most cases (s. Tables 4–6).
4) When $E_I/E_M < 1$, the maximum stress is σ_θ appearing at $\psi = \pm 90$, which in most cases varies more than twice in the range $b/d = 0 - 0.9$. On the other hand, when $E_I/E_M > 1$, the

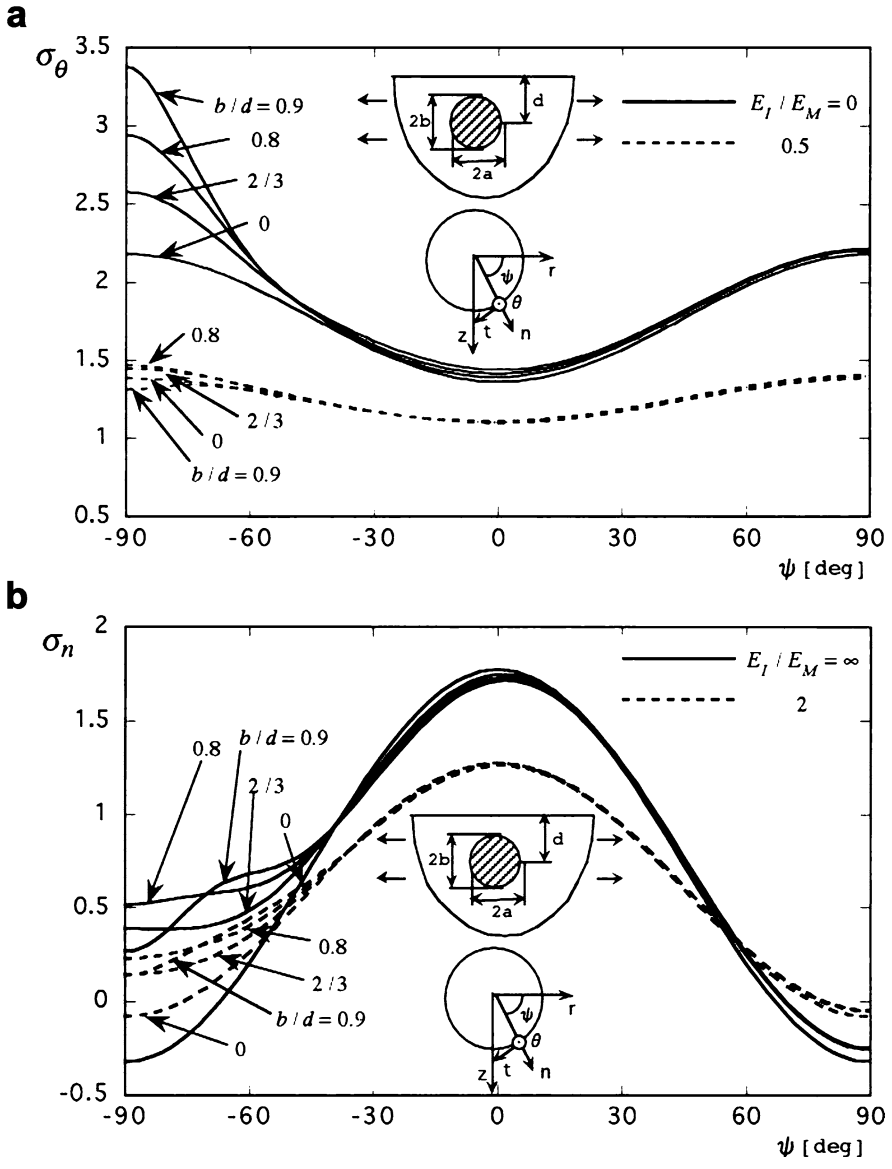

Fig. 4a, b. Interface stress for $a/b = 1$ **a** σ_θ for $E_I/E_M < 1$; **b** σ_n for $E_I/E_M > 1$

maximum stresses is σ_n appearing at $\psi = 0$, which varies only 8% at the most. In the latter case, the effect of the free surface is comparatively small (s. Table 7, Fig. 4).

Appendix

The fundamental stress and displacement fields are given by the following equations when ring forces are acting in the r- and z-directions in a semi-infinite body:

$$K_{nn}^{Fr} = \sigma_n^{Fr} = \sigma_r^{Fr}\cos^2\psi + \sigma_z^{Fr}\sin^2\psi + 2\tau_{rz}^{Fr}\cos\psi\sin\psi,$$

$$K_{nn}^{Fz} = \sigma_n^{Fz} = \sigma_r^{Fz}\cos^2\psi + \sigma_z^{Fz}\sin^2\psi + 2\tau_{rz}^{Fz}\cos\psi\sin\psi,$$

$$K_{nt}^{Fr} = \tau_{nt}^{Fr} = \left(\sigma_z^{Fr} - \sigma_r^{Fr}\right)\cos\psi\sin\psi + 2\tau_{rz}^{Fr}\left(\cos^2\psi - \sin^2\psi\right),$$

$$K_{nt}^{Fz} = \tau_{nt}^{Fz} = \left(\sigma_z^{Fz} - \sigma_r^{Fz}\right)\cos\psi\sin\psi + 2\tau_{rz}^{Fz}\left(\cos^2\psi - \sin^2\psi\right). \qquad \text{(A1)}$$

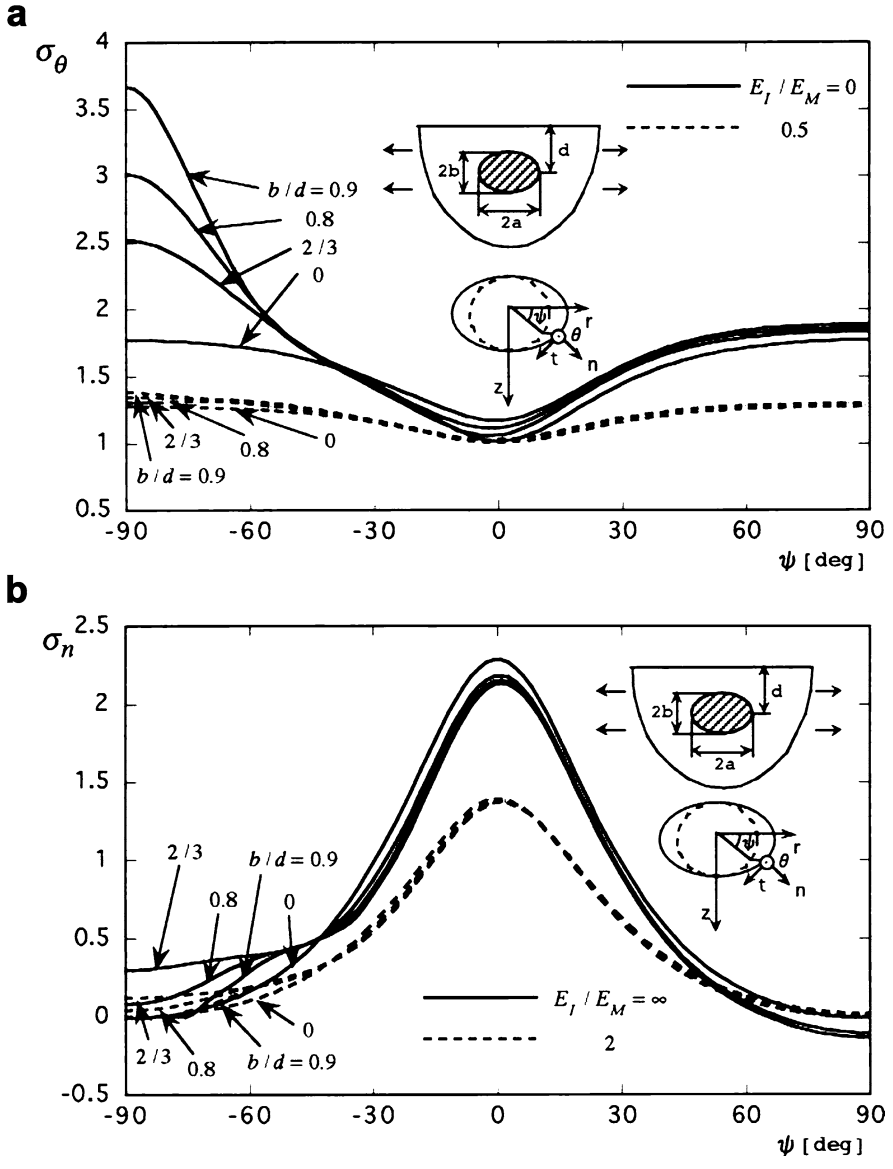

Fig. 5a, b. Interface stress for $a/b = 2$ **a** σ_θ for $E_I/E_M < 1$; **b** σ_n for $E_I/E_M > 1$

$$K_{ur}^{F_r} = U_r^{F_r} = A\Big[r_m^2(3-4v)I_{1,1} - \{r\rho I_{3,0} - (r^2+\rho^2)I_{3,1} + r\rho I_{3,2}\} + r_m^2 J_{1,1} - (3-4v)\{r\rho J_{3,0} - (r^2+\rho^2)J_{3,1} + r\rho J_{3,2}\} + 2z\zeta J_{3,1} - \frac{6z\zeta}{r_m^2}\{r\rho J_{5,0} - (r^2+\rho^2)J_{5,1} + r\rho J_{5,2}\}\Big] + A\int_0^\pi \frac{4(1-v)(1-2v)}{(R_2+z+\zeta)}\left[\cos\varphi - \frac{(r\cos\varphi-\rho)(r-\rho\cos\varphi)}{R_2(R_2+z+\zeta)}\right]d\varphi, \tag{A2}$$

$$K_{uz}^{Fr} = U_z^{F_r} = A\Big[-(z-\zeta)(\rho I_{3,0} - rI_{3,1}) - (3-4v)(z-\zeta)(\rho J_{3,0} - rJ_{3,1}) + \frac{6z\zeta}{r_m^2}(z+\zeta)(\rho J_{5,0} - rJ_{5,1})\Big] - A\int_0^\pi \frac{4(1-v)(1-2v)(\rho - r\cos\varphi)}{R_2(R_2+z+\zeta)}d\varphi, \tag{A3}$$

$$K_{ur}^{F_z} = U_r^{F_z} = A\Big[(z-\zeta)(rI_{3,0} - \rho I_{3,1}) + (3-4v)(z-\zeta)(rJ_{3,0} - \rho J_{3,1}) + \frac{6z\zeta}{r_m^2}(z+\zeta)(rJ_{5,0} - \rho J_{5,1})\Big] - A\int_0^\pi \frac{4(1-v)(1-2v)}{R_2(R_2+z+\zeta)}(r-\rho\cos\varphi)d\varphi, \tag{A4}$$

Table 7. Position and maximum stress in the matrix due to an ellipsoidal inclusion, comp. Fig. 1

a/b	b/d	$E_I/E_M = 0$		$E_I/E_M = 0.5$		$E_I/E_M = 2$		$E_I/E_M = \infty$	
		ψ (deg.)	σ_θ	ψ (deg.)	σ_θ	ψ (deg.)	σ_n	ψ (deg.)	σ_n
1/2	0	±90	2.537	±90	1.449	0	1.208	0	1.533
	1/3	−90	2.545	−90	1.450	−0.1	1.207	−0.1	1.532
	1/2	−90	2.575	−90	1.454	−0.1	1.207	−0.1	1.529
	2/3	−90	2.663	−90	1.468	0	1.206	0	1.524
	0.8	−90	2.832	−90	1.508	0.4	1.205	0.7	1.518
	0.9	−90	3.076	−90	1.549	1.0	1.204	1.2	1.511
1	0	±90	2.182	±90	1.384	0	1.275	0	1.775
	1/3	−90	2.216	−90	1.388	0.1	1.274	0.2	1.770
	1/2	−90	2.326	−90	1.404	0.3	1.274	0.7	1.761
	2/3	−90	2.579	−90	1.448	0.6	1.273	1.3	1.752
	0.8	−90	2.948	−90	1.468	0.8	1.268	1.7	1.732
	0.9	−90	3.385	−90	1.405	0.8	1.261	1.9	1.716
2	0	±90	1.773	±90	1.279	0	1.392	0	2.288
	1/3	−90	1.890	−90	1.296	0.3	1.390	0.2	2.259
	1/2	−90	2.137	−90	1.335	0.5	1.387	0.4	2.227
	2/3	−90	2.519	−90	1.349	0.7	1.380	0.5	2.184
	0.8	−90	3.014	−70	1.318	0.9	1.373	0.8	2.151
	0.9	−90	3.669	−90	1.387	1.0	1.369	1.0	2.134

$$K_{uz}^{F_z} = U_z^{F_z} = A\Big[r_m^2(3-4\nu)I_{1,0} + (z-\zeta)^2 I_{3,0} + r_m^2\big\{8(1-\nu)^2 - (3-4\nu)\big\}J_{1,0}$$
$$-(3-4\nu)\big\{(3-4\nu)(z+\zeta)^2 - 2z\zeta\big\}J_{3,0} + \frac{6z\zeta}{r_m^2}(z+\zeta)^2 J_{5,0}\Big], \tag{A5}$$

$$\sigma_r^{F_r} = B\Big[-(1-2\nu)(\rho I_{3,0} + rI_{3,1} - 2\rho I_{3,2})$$
$$+\frac{3}{r_m^2}\big\{r^2\rho I_{5,0} - r\big(r^2+2\rho^2\big)I_{5,1} + \rho\big(2r^2+\rho^2\big)I_{5,2} - r\rho^2 I_{5,3}\big\}$$
$$-(1-2\nu)\big\{(3-4\nu)\rho J_{3,0} - (5-4\nu)rJ_{3,1} + 2\rho J_{3,2}\big\}$$
$$+\frac{3}{r_m^2}(3-4\nu)\big\{r\rho^2 J_{5,0} - r\big(r^2+2\rho^2\big)J_{5,1} + \rho\big(2r^2+\rho^2\big)J_{5,2} - r\rho^2 J_{5,3}\big\}$$
$$+\frac{6\zeta}{r_m^2}\{(1-2\nu)(z+\zeta) - \zeta\}\big(\rho J_{5,0} - rJ_{5,1}\big) - \frac{12z\zeta}{r_m^2}\big(rJ_{5,1} - \rho J_{5,2}\big)$$
$$-\frac{30}{r_m^4}\big\{r^2\rho J_{7,0} - r\big(r^2+2\rho^2\big)J_{7,1} + \rho\big(2r^2+\rho^2\big)J_{7,2} - r\rho^2 J_{7,3}\big\}\Big]$$
$$+B\int_0^\pi \frac{4(1-\nu)(1-2\nu)}{R_2(R_2+z+\zeta)^2}\Big[2\rho - 3r\cos\varphi + \rho\cos^2\varphi$$
$$+\frac{3R_2+z+\zeta}{R_2^2(R_2+z+\zeta)}(r-\rho\cos\varphi)^2(r\cos\varphi-\rho)\Big]d\varphi, \tag{A6}$$

$$\sigma_z^{F_r} = B\Big[-(1-2\nu)(\rho I_{3,0} - rI_{3,1}) + \frac{3}{r_m^2}(z-\zeta)^2\big(\rho I_{5,0} - rI_{5,1}\big) + (1-2\nu)\big(\rho J_{3,0} - rJ_{3,1}\big)$$
$$+\frac{3}{r_m^2}(3-4\nu)(z+\zeta)^2\big(\rho J_{5,0} - rJ_{5,1}\big) - \frac{6\zeta}{r_m^2}\{\zeta + (1-2\nu)(z+\zeta)\}\big(\rho J_{5,0} - rJ_{5,1}\big)$$
$$-\frac{30z\zeta}{r_m^4}(z+\zeta)^2\big(\rho J_{7,0} - rJ_{7,1}\big)\Big], \tag{A7}$$

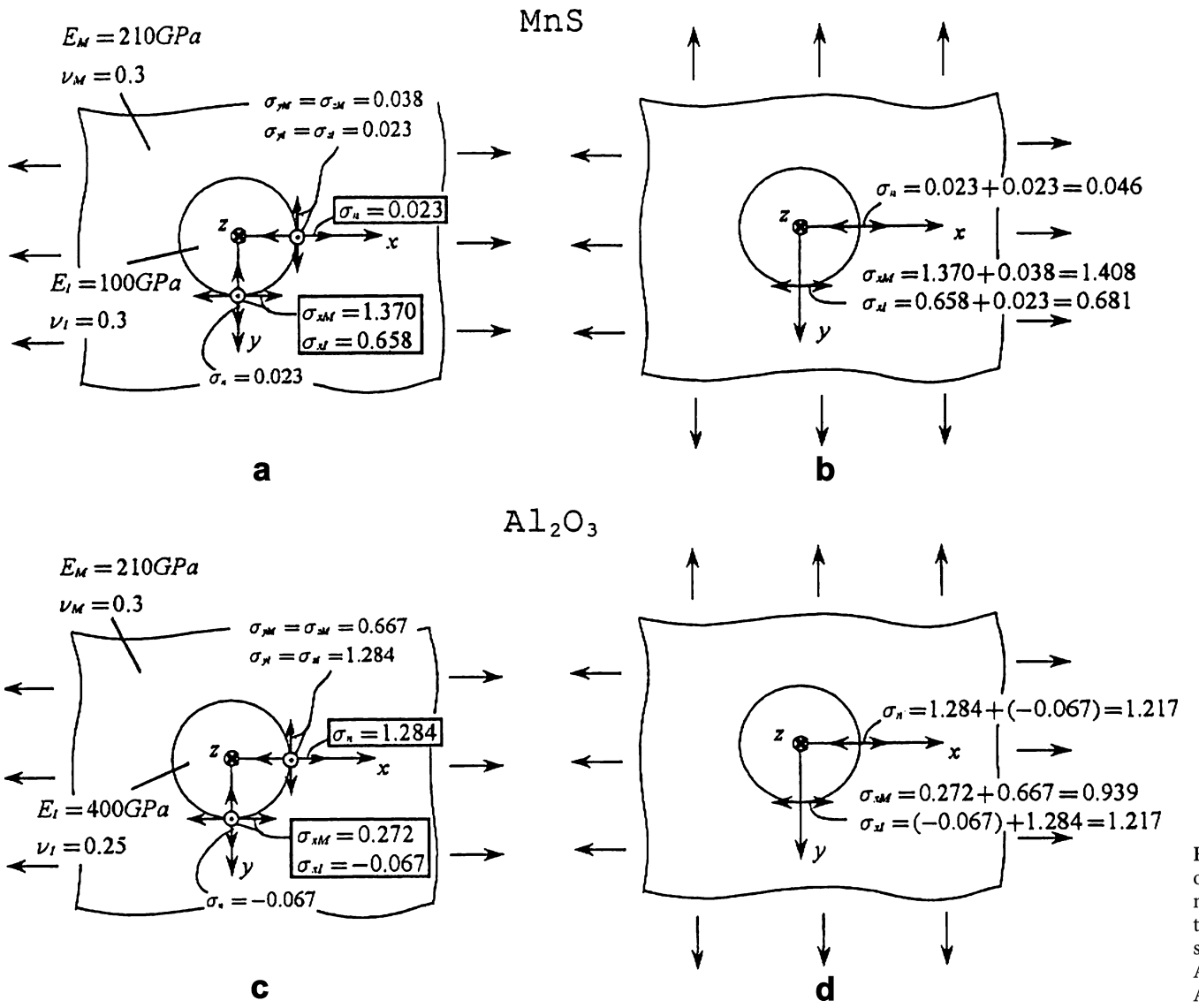

Fig. 6a, b, c, d. Stress concentration of a spheroidal inclusion in an infinite body under uniaxial or biaxial tension **a** MnS under uniaxial tension, **b** MnS under biaxial tension, **c** Al_2O_3 under uniaxial tension, **d** Al_2O_3 under biaxial tension

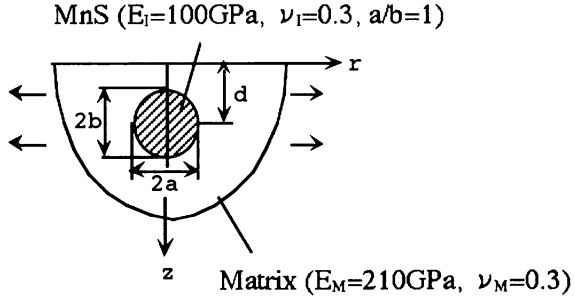

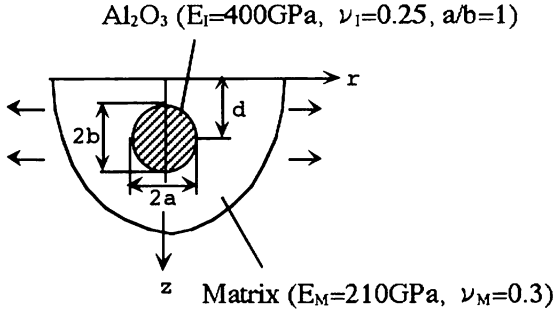

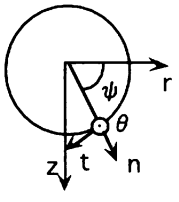

Fig. 7. A spheroidal inclusion of MnS or Al_2O_3 in the matrix of a high-strength steel

$$\begin{aligned}\sigma_\theta^{F_r} = B\Big[&(1-2v)(\rho I_{3,0} + rI_{3,1} - 2\rho I_{3,2}) + \frac{3}{r_m^2}\left(\rho I_{5,0} - rI_{5,1} - \rho I_{5,2} + rI_{5,3}\right)\\ &- (1-2v)\left\{(5-4v)\rho J_{3,0} - (3-4v)rJ_{3,1} - 2\rho J_{3,2}\right\}\\ &+ \frac{3}{r_m^2}(3-4v)\rho^2\left(\rho J_{5,0} - rJ_{5,1} - \rho J_{5,2} + rJ_{5,3}\right) + \frac{6z\zeta}{r_m^2}\left(3\rho J_{5,0} - rJ_{5,1} - 2\rho J_{5,2}\right)\\ &- \frac{12v\zeta}{r_m^2}(z+\zeta)\left(\rho J_{5,0} - rJ_{5,1}\right) - \frac{30}{r_m^4}\rho^2 z\zeta\left(\rho J_{7,0} - rJ_{7,1} - \rho J_{7,2} + rJ_{7,3}\right)\Big]\\ &+ B\int_0^\pi \frac{4(1-v)(1-2v)}{R_2(R_2+z+\zeta)^2}\Big[3\rho + r\cos\varphi + 2\rho\cos^2\varphi\\ &+ \frac{3R_2+z+\zeta}{R_2^2(R_2+z+\zeta)}\rho^2(r\cos\varphi - \rho)\left(1-\cos^2\varphi\right)\Big]d\varphi, \end{aligned} \tag{A8}$$

$$\begin{aligned}\tau_{rz}^{F_r} = B\Big[&-(1-2v)(z-\zeta)I_{3,1} + \frac{3}{r_m^2}(z-\zeta)\left\{r\rho I_{5,0} - \left(r^2+\rho^2\right)I_{5,1} + r\rho I_{5,2}\right\}\\ &+ (1-2v)(z-\zeta)J_{3,1} + \frac{3}{r_m^2}(3-4v)(z+\zeta)\left\{r\rho J_{5,0} - \left(r^2+\rho^2\right)J_{5,1} + r\rho J_{5,2}\right\}\\ &- \frac{6\zeta}{r_m^2}(1-2v)\left\{r\rho J_{5,0} - \left(r^2+\rho^2\right)J_{5,1} + r\rho J_{5,2}\right\} - \frac{6\zeta z}{r_m^2}(z+\zeta)J_{5,1}\\ &- \frac{30z\zeta}{r_m^2}(z+\zeta)\left\{r\rho J_{7,0} - \left(r^2+\rho^2\right)J_{7,1} + r\rho J_{7,2}\right\}\Big], \end{aligned} \tag{A9}$$

Table 8. Position and maximum stress due to a spheroidal inclusion of MnS or Al_2O_3 in the matrix of a high-strength steel, comp Fig. 7

b/d	MnS		Al_2O_3	
	ψ (deg.)	σ_θ	ψ (deg.)	σ_n
0	±90	1.408	0	1.217
0.1	−90	1.408	0	1.217
0.3	−90	1.412	0.1	1.217
0.4	−90	1.418	0.2	1.216
0.5	−90	1.431	0.3	1.216
0.8	−90	1.503	0.8	1.216
0.9	90	1.431	0.9	1.210

$$\sigma_r^{F_z} = B\Big[(1-2v)(z-\zeta)I_{3,0} - \frac{3}{r_m^2}(z-\zeta)\{r^2I_{5,0} - 2r\rho I_{5,1} + \rho^2 I_{5,2}\}$$
$$+ (1-2v)\{3(z-\zeta) - 4v(z+\zeta)\}J_{3,0} - \frac{3}{r_m^2}(3-4v)(z-\zeta)\{r^2J_{5,0} - 2r\rho J_{5,1} + \rho^2 J_{5,2}\}$$
$$+ \frac{6\zeta}{r_m^2}(z+\zeta)\{z-2v(z+\zeta)\}J_{5,0} - \frac{30z\zeta}{r_m^4}(z+\zeta)\{r^2J_{5,0} - 2r\rho J_{5,1} + \rho^2 J_{5,2}\}\Big]$$
$$+ B\int_0^\pi \frac{4(1-v)(1-2v)}{R_2(R_2+z+\zeta)}\left[1 - \left\{\frac{1}{R_2(R_2+z+\zeta)} + \frac{1}{R_2^2}\right\}(r-\rho\cos\varphi)^2\right]d\varphi, \qquad \text{(A10)}$$

$$\sigma_z^{F_z} = B\Big[-(1-2v)(z-\zeta)I_{3,0} - \frac{3}{r_m^2}(z-\zeta)^3 I_{5,0} + (1-2v)(z-\zeta)J_{3,0}$$
$$+ \frac{3}{r_m^2}\{(3-4v)z(z+\zeta)^2 - \zeta(z+\zeta)(5z-\zeta)\}J_{5,0} - \frac{30z\zeta}{r_m^4}(z+\zeta)^3 J_{7,0}\Big], \qquad \text{(A11)}$$

$$\sigma_\theta^{F_z} = B\Big[(1-2v)(z-\zeta)I_{3,0} - \frac{3\rho^2}{r_m^2}(z-\zeta)(I_{5,0} - I_{5,2}) + (1-2v)\{3(z-\zeta) - 4v(z+\zeta)\}J_{3,0}$$
$$- \frac{3}{r_m^2}(3-4v)\rho^2(z-\zeta)(J_{5,0} - J_{5,2}) + \frac{6\zeta}{r_m^2}(z+\zeta)\{z-2v(z+\zeta)\}J_{5,0}$$
$$- \frac{30\rho^2 z\zeta}{r_m^4}(z+\zeta)(J_{7,0} - J_{7,2})\Big]$$
$$- B\int_0^\pi \frac{4(1-v)(1-2v)}{R_2(R_2+z+\zeta)}\left[1 - \left\{\frac{1}{R_2(R_2+z+\zeta)} + \frac{1}{R_2^2}\right\}\rho^2(1-\cos^2\varphi)\right]d\varphi, \qquad \text{(A12)}$$

$$\tau_{rz}^{F_z} = B\Big[-(1-2v)(rI_{3,0} - \rho I_{3,1}) - \frac{3}{r_m^2}(z-\zeta)^2(rI_{5,0} - \rho I_{5,1}) + (1-2v)(rJ_{3,0} - \rho J_{3,1})$$
$$- \frac{3}{r_m^2}\{(3-4v)z(z+\zeta) - \zeta(3z+\zeta)\}(rJ_{5,0} - \rho J_{5,1}) - \frac{30z\zeta}{r_m^4}(z+\zeta)^2(rJ_{7,0} - \rho J_{7,1})\Big], \qquad \text{(A13)}$$

where

$$I_{n,m} = \int_0^{\pi/2} \frac{\cos^m\varphi}{(e_1 - \cos\varphi)^{n/2}}d\varphi,$$
$$J_{n,m} = \int_0^{\pi/2} \frac{\cos^m\varphi}{(e_2 - \cos\varphi)^{n/2}}d\varphi,$$
$$A = \frac{\rho}{8\pi G(1-v)r_m^3},$$

$$B = \frac{\rho}{4\pi G(1-\nu)r_m^3}$$

$$e_1 = 1 + \frac{(r-\rho)^2+(z-\zeta)^2}{2r\rho},$$

$$e_2 = 1 + \frac{(r-\rho)^2+(z+\zeta)^2}{2r\rho},$$

$$r_m = \sqrt{2r\rho},$$

$$R_2^2 = r^2 + \rho^2 + (z+\zeta)^2 - 2r\rho\cos\varphi.$$

Here, $I_{n,m}$ and $J_{n,m}$ $(n = 3,\ 5,\ 7, \quad m = 0,\ 1,\ 2,\ 3)$ can be expressed by using complete elliptic integrals, [30, 31].

References

1. **Mitchell, M.R.:** Review on the mechanical properties of cast steels with emphasis on fatigue behavior and influence of microdiscontinuities. ASME, J. Eng. Mat. Tech: (1977) 329–343
2. **Murakami, Y:** Metal fatigue: effect of small defects and nonmetallic inclusions. Elsevier, 2002
3. **Edwards, R.H.:** Stress concentrations around spherical inclusions and cavities. Trans. ASME, J. Appl. Mech. 19(1) (1952) 19–30
4. **Eshelby, J.D.:** The determination of the elastic field of an ellipsoidal inclusion and related problems. Proc R Soc A 241 (1957) 376–396
5. **Eshelby, J.D.:** The elastic field outside an ellipsoidal inclusion. Proc R Soc A 252 (1959) 561–569
6. **Donnel, L.H.:** Stress concentration due to elliptical discontinuities in plates under edge forces. Annual vol. T. Von Karman, Calif Inst Tech (1941) 293–309
7. **Nisitani, H.:** Approximate calculation method of interaction between notches and its applications. J. JSME (in Japanese) 70 589 (1968) 35–47
8. **Shioya, S.:** Tension of an infinite thin plate having two rigid spherical inclusions. Trans. JSME (in Japanese) 36 (1970) 886–897
9. **Isida, M.; Igawa, H.:** Some asymtotic behaviour and formulate of stress intensity factors for a collinear and parallel cracks under various loadings. Int J Fracture 65 (1994) 247–259
10. **Noda, N.-A.; Matsuo, T.:** Analysis of a row of elliptical inclusions in a plate using singular integral equations. Int J Fracture 83 (1997) 315–336
11. **Miyamoto, H.:** On the problem of the theory of elasticity for a region containing more than two spherical cavities. Trans JSME (in Japanese) 23(131) (1957) 431–436
12. **Nisitani, H.:** On the tension of an elastic body having an infinite row of spheroidal cavities. Trans JSME (in Japanese) 29(200) (1963) 765–768
13. **Eubank, R.A.:** Stress interference in three-dimensional torsion. Trans. ASME J Appl Mech 32(1) (1956) 21–25
14. **Shelly, J.F.; Yu, Yi-Yuan.:** The effect of two rigid spherical inclusions on the stresses in an infinite elastic solids. Trans ASME J Appl Mech 33(1) (1966) 68–74
15. **Tsuchida, E.; Nakahara, I.; Kodama, M.:** Asymmetric problem of elastic body containing several spherical cavities (first report: two spherical cavities in an elastic body). Trans Jpn Soc Mech Engrs (JSME) 42 (1976) 46–54 (in Japanese)
16. **Noda, N.-A.; Hayashida, H.; Tomari, K.:** Interaction among a row of ellipsoidal inclusions. Int J Fracture 102 (2000) 371–392
17. **Noda, N.A.; Ogasawara, N.; Matsuo, T.:** Asymmetric problem of a row of revolutional ellipsoidal cavities using singular integral equations. Int J Solids and Struct 40(8) (2003) 1923–1941
18. **Tsuchida, E.; Nakahara, I:** Three-dimensional stress concentration around a spherical cavity in a semi-infinite elastic body. Bull JSME, 13 (1970).499–508
19. **Tsuchida, E.; Nakahara, I.:** Stresses in a semi-infinite body subjected to uniform pressure on the surface of a cavity and the plane boundary. Bull JSME, 15 (1972) 1–10
20. **Tsuchida, E.; Nakahara, I.:** Stress concentration around a spheroidal cavity in a semi-infinite elastic body under uni-axial tension. Trans Japan Soc Mech Eng 40 (1974) 285–297 (in Japanese)
21. **Tsuchida, E.; Nakahara, I.; Kodama, M.:** Stress concentration around a prolate spheroidal cavity in a semi-infinite elastic body under all-around tension. Bull JSME, 25(202) (1982) 493–500
22. **Jasiuk, I.; Sheng, P.Y.; Tsuchida, E.:** A spherical inclusion in an elastic half-space under shear. Trans. ASME, J Appl Mech 64 (1997) 471–479
23. **Nisitani, H.:** The two-dimensional stress problem solved using sn electric digital computer. J Japanese Soc Mech Eng 70 (1967) 627–632 [(1969), Bulletin of Japanese Society of Mechanical Engineering 11: 14–23.]
24. **Noda, N.-A.; Matsuo, T.:** Singular integral equation method in optimization of stress-relieving hole: a new approach based on the body force method. Int J Fracture 70 (1995) 147–165
25. **Noda, N.A.; Matsuo, T.:** Numerical solution of singular integral equations in stress concentration problems. Int J Solids and Struct 34 (1997) 2429–2444

26. **Noda, N.A.; Matsuo, T.:** Singular integral equation method for interaction between elliptical inclusions. Trans. ASME 65 (1998) 310–319
27. **Mindlin, R.D.:** Force at point in the interior of a semi-infinite solid. Physics 7 (1974) 195–202
28. **Murakami, Y.; Zhou, S.:** Analysis of stress/strain concentration at nonmetallic inclusion and S-N curve of ultra-long fatigue failure of high-strength steels. Transactions of Japan Soc Mech Engineers 68 (2002) 26–34 (in Japanese)
29. **Brooksbank, D.; Andrews, K.W.:** Stress fields around inclusions and their relation to mechanical properties. J Iron Steel Inst 210 (1972) 246–255
30. **Nisitani, H.; Noda, N.-A.:** Tension of a cylindrical bar having an infinite row of circumferential cracks. Eng Fracture Mech 20(4) (1984) 675–686
31. **Nisitani, H.; Noda, N.-A.:** Stress concentration of a cylindrical bar with a V-shaped circumferential groove under torsion, tension or bending. Eng Fracture Mech 20(5/6) (1984) 743–766